iJRASET
International Journal For Research in Applied Science and Engineering Technology

INTERNATIONAL JOURNAL FOR RESEARCH

IN APPLIED SCIENCE & ENGINEERING TECHNOLOGY

Volume: 13 **Issue:** III **Month of publication:** March 2025

DOI: https://doi.org/10.22214/ijraset.2025.68891

www.ijraset.com

Call: 08813907089 | E-mail ID: ijraset@gmail.com

International Journal for Research in Applied Science & Engineering Technology (IJRASET)
ISSN: 2321-9653; IC Value: 45.98; SJ Impact Factor: 7.538
Volume 13 Issue III Mar 2025- Available at www.ijraset.com

Quantum Chemical and Reactivity-Based Evaluation of Aspartic Acid and its Oligomers as Eco-Friendly Corrosion Inhibitors for Iron Surfaces

Babatunde T. Ogunyemi
Physical and computational unit, Department of Chemistry, Federal University Otuoke, Bayelsa State

Abstract: ***This study investigates the corrosion inhibition potential of aspartic acid (ASP) and oligomers on iron surfaces through quantum chemical calculations. Aspartic acid monomer (ASP), dimer (DASP), and trimer (TASP) were analyzed using density functional theory at the B3LYP/6-31G(d) level to determine their electronic properties and reactivity patterns. Quantum chemical parameters including HOMO-LUMO energies, energy gap, dipole moment, softness, hardness, and electrophilicity were calculated to elucidate structure-activity relationships. Results revealed a progressive decrease in energy gap values (ASP: 7.12 eV → DASP: 6.12 eV → TASP: 6.05 eV), indicating enhanced chemical reactivity with increasing molecular size. HOMO energies demonstrated an increasing trend from ASP (-6.89 eV) to TASP (-6.48 eV), suggesting improved electron-donating capability in larger molecules. Fukui function analysis identified specific reactive sites, with oxygen atoms exhibiting strong electrophilic character as evidenced by significant negative f_k^- values, particularly at carbonyl groups. The distribution of reactive sites became more dispersed with increasing molecular size, potentially enabling multiple points of interaction with metal surfaces. These findings suggest that larger PASP oligomers may provide superior corrosion inhibition through enhanced electron transfer capabilities, stronger dipole interactions, and more distributed reactive sites for surface adsorption. This computational study provides valuable insights for the rational design of environmentally friendly corrosion inhibitors based on aspartic acid and oligomers.***

Keywords: Density Functional Theory; Biomolecule; corrosion inhibition, Aspartic acid

I. INTRODUCTION

Metallic corrosion remains one of the most pressing challenges for global infrastructure, costing economies over $2.5 trillion annually which is about nearly 3.4% of the world's GDP (Koch et al., 2016). Beyond the staggering financial toll, corrosion accelerates resource depletion and environmental harm, as failed structures demand frequent replacements. This accelerated degradation leads to increased raw material consumption, increased carbon emissions from production and transport, and potential environmental contamination from the release of corrosion products. Iron and its alloys, though indispensable in industries, are especially vulnerable in harsh environments, making effective protection strategies critical (Novák et al., 2021). Corrosion protection strategies such as coatings, inhibitors, and material choice to combat degradation, enhances structural durability, reducing costs, and preventing failures (Kumari et al., 2024). Chemical inhibitors have long been a practical choice for mitigating corrosion. However, traditional options like chromates and phosphate-based compounds are increasingly restricted due to their toxicity and environmental persistence (Răuță et al., 2025; Sandeep et al., 2024). This regulatory shift has spurred interest in eco-friendly alternatives that balance high performance with minimal ecological impact.

Amino acids, such as aspartic acid, stand out as promising candidates. Naturally occurring and biodegradable, they offer a sustainable solution without sacrificing efficiency (Verma et al., 2023; El Ibrahimi 2020; Chauhan et al., 2021). Their efficiency can be enhanced through chemical modifications or the use of synergists, ensuring effective corrosion protection. Aspartic acid, in particular, intrigues researchers due to its molecular structure. With both carboxyl and amino groups, it can bind to metal surfaces through multiple interaction sites, forming protective layers (Zhang et al., 2018). When polymerized, its oligomers may enhance this ability, creating denser protective films through cooperative adsorption. This feature could significantly boost corrosion resistance.

Recent experiments highlight amino acids' potential, showing strong inhibition on iron surfaces via adsorption-driven protective films (El Ibrahimi 2020; Răuță et al., 2025).

Yet, the exact mechanisms behind aspartic acid's interactions with iron remain unclear at the molecular level. While electrochemical studies suggest concentration-dependent efficiency, these findings don't fully explain the electronic or structural factors at play (El-Hajjaji et al., 2018).

Computational methods like quantum chemical calculations are bridging this gap. By analyzing electronic properties, researchers can predict performance and design better inhibitors (Ogunyemi et al., 2020; Guo et al., 2017). Parameters such as molecular orbital energies and reactivity indices help correlate structure with function, offering a roadmap for optimization (Ogunyemi et al., 2020; Obot et al., 2019). Through computational method, correlation between the properties of inhibiting molecules with their inhibition efficiencies has been established (Oyebamiji et al., 2018). Also, quantitative structure property relationships (QSPRS) for various sets of inhibiting molecules have been derived (Ogunyemi et al., 2020; Bereket et al., 2002), in order to find a consistent relationship between the changes in quantum molecular properties and inhibitor efficiency for a set of inhibitors.

Despite aspartic acid's potential, comprehensive studies on its electronic behavior and adsorption dynamics are scarce. Without this knowledge, it's challenging to refine these compounds for real-world use or fully exploit their environmental benefits. This study addresses that gap by systematically evaluating aspartic acid and its oligomers as iron corrosion inhibitors. Using quantum chemical analyses and reactivity assessments, we explore their electronic structures, and adsorption patterns. We hypothesize that oligomerization enhances performance through cooperative binding and that specific electronic parameters strongly predict efficiency. By linking molecular features to function, this work aims to guide the design of greener inhibitors while deepening our understanding of corrosion prevention at the atomic scale.

II. METHODOLOGY

A. *Computational Details*

Molecular modeling techniques offer a powerful approach to interpret experimental data and predict the behavior of new materials relevant to industrial applications. In this study, we performed all quantum chemical calculations using the Spartan 14 software package under standard conditions (298.15 K, 1 atm) for isolated gaseous systems. To model aspartic acid and its oligomers (dimer, trimer, tetramer), we employed density functional theory (DFT) with the B3LYP hybrid functional and the 6-311++G(d,p) basis set. This combination strikes a balance between computational efficiency and accuracy, as demonstrated in prior studies of organic inhibitors (Verma et al., 2023). After structural optimization, frequency calculations confirmed that each geometry corresponded to a true energy minimum, with no imaginary frequencies detected.

To evaluate corrosion inhibition potential, we calculated key quantum chemical parameters linked to molecular reactivity. These included the energies of the highest occupied (HOMO) and lowest unoccupied (LUMO) molecular orbitals, which reflect a molecule's electron-donating and -accepting tendencies. The HOMO-LUMO energy gap (ΔE) served as an indicator of stability and reactivity. Smaller gaps typically correlate with higher inhibition efficiency (Guo et al., 2017).

B. *Global Reactivity Descriptors Calculation*

Global reactivity descriptors were computed using Koopmans' theorem and finite difference approximations. These parameters included electronegativity (χ), global hardness (η), global softness (σ), and the fraction of electrons transferred (ΔN) from the inhibitor molecule to the iron surface. The electron affinity (EA) and ionization potential (IP) of the studied inhibitors were related to the E_{HOMO} and E_{LUMO} (equation 1 and 2) using Koopman's theorem (Pearson, *et al.,* 1988) to calculate the absolute hardness and chemical potential (μ) values of the organic inhibitors as shown in equations 3 and 4.

$$IP = -E_{HOMO} \quad (1)$$

$$EA = -E_{LUMO} \quad (2)$$

$$\eta = \left(\frac{\delta\varepsilon^2}{\delta N^2}\right)_{v(r)} = \frac{E_{LUMO} + E_{HOMO}}{2} = \frac{IP - EA}{2} \quad (3)$$

$$-\mu = \chi = \left(\frac{\delta\varepsilon}{\delta N}\right)_{v(r)} = -\frac{E_{LUMO} + E_{HOMO}}{2} = \frac{IP + EA}{2} \quad (4)$$

Electronegativity was calculated as the negative of the chemical potential (μ), while global softness was computed as the reciprocal of global hardness (Obot & Obi-Egbedi, 2011; Ogunyemi et al., 2020) as shown in equation 5.

$$S = \frac{1}{\eta} \quad (5)$$

The three quantum parameters of organic inhibitors: softness, electronegativity and hardness are very helpful in examining their chemical reactivity.

The electron transfer fraction (ΔN) was calculated using equation 6. The theoretical value of 7.0 eV for the electronegativity of iron and assuming a global hardness of zero for the bulk metal, following the approach described by Pearson 1988).

$$\Delta N = \frac{\chi_{Fe} - \chi_{inh}}{2(\eta_{Fe} + \eta_{inh})} \qquad (6)$$

χ_{Fe} and χ_{inh} represent the absolute electronegativities of iron (Fe) and organic inhibitor while η_{Fe} and η_{inh} represent the hardness of iron (Fe) and inhibitor respectively.

The value of back donation of charges was calculated using the following expression:

$$\Delta E_{(Back-donation)} = \frac{\mu}{4}$$

The electrophilicity index parameter of each of the molecules was estimated using equation 7 (Parr *et al*., 1999). This property measures the stabilization energy when charges are transferred to a system from the environment. It also measures the tendency of chemical species to accept electrons.

$$\omega = \frac{\mu^2}{2\eta} \qquad (7)$$

When the values of μ and ω are low, it shows that inhibiting molecules is a more reactive nucleophile while high values depict a more reactive electrophile.

Local reactivity was assessed through Fukui indices, computed via Mulliken population analysis of neutral, cationic, and anionic species. using the optimized geometries. Condensed Fukui functions for nucleophilic (f_k^+) and electrophilic (f_k^-) attacks were computed based on the Mulliken population analysis. The partial atomic charge is defined by qk(N+1) when a molecule accepts electron and by qk(N-1) when it loses an electron. For a neutral molecule, the charge on each atom is defined by qk(N). The nucleophilic, electrophilic and dual Fukui parameters were calculated using Yao's dual descriptors as shown in Eqs. 8, 9 and 10, respectively.

$f_k^+ = [q_k(N+1) - q_k(N)]$ nucleophilic attack 8

$f_k^- = [q_k(N) - q_k(N-1)]$ electrophilic attack 9

$\Delta f_k(r) = f_k^+ - f_k^-$ 10

These indices pinpointed regions prone to nucleophilic or electrophilic interactions and offers insights into potential binding sites. Molecular electrostatic potential (MEP) maps further visualized charge distribution, highlighting areas likely to engage with iron surfaces (Wazzan & Mahgoub, 2014).

III. RESULTS AND DISCUSSION

A. Quantum Chemical Molecular Descriptors

The theoretical investigation of Polyaspartic Acid (Table 1) explores their potential as corrosion inhibitors using DFT/B3LYP/6-31G* methods. The molecular and optimized structures of the inhibitors are illustrated (Figure 1), revealing the addition of monomer to the monomeric ASP to form the di- and tri- ASP.

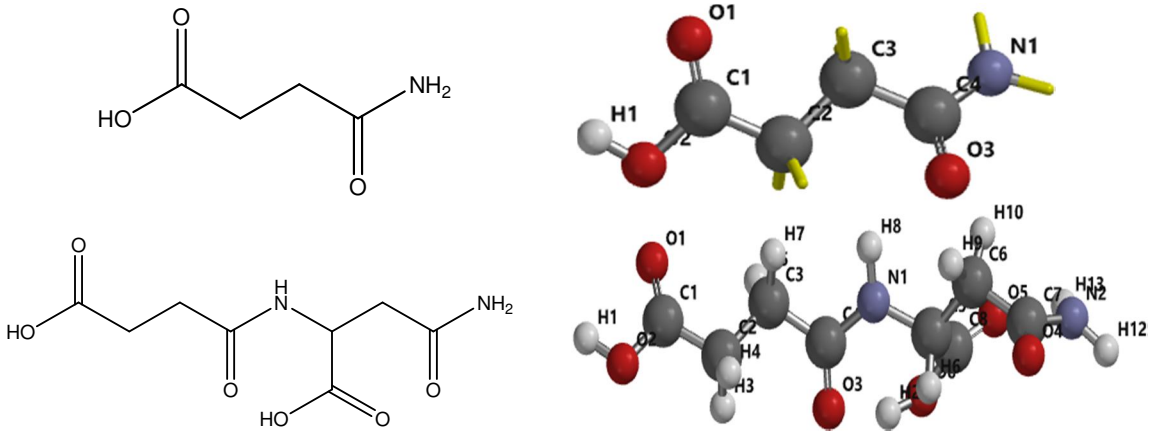

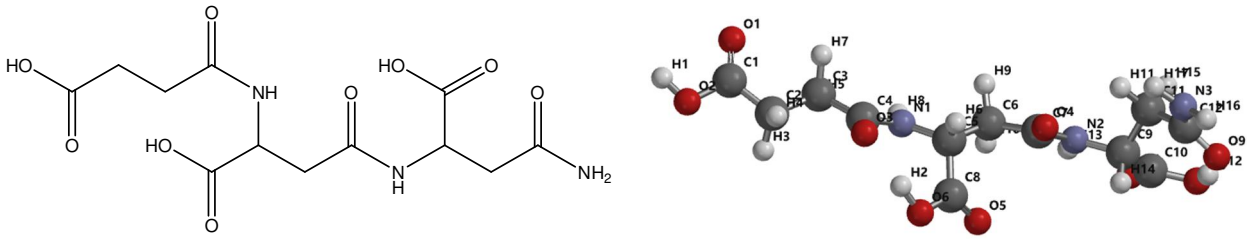

Figure 1. Molecular and optimized structures of the studied inhibitors

Various quantum chemical parameters such as E_{HOMO}, E_{LUMO}, energy gap ΔE, dipole moment (DM), Log P, solvation energy (E_{solv}), Ovality, electron affinity (EA), ionization potential (IP), global electrophilicity (ω), softness (s), chemical hardness (η), electronegativity (χ), molecular weight (MW), electron transfer energy ΔN, and polarizability are meticulously calculated and displayed in Table 1.

The HOMO and LUMO energies provide crucial insights into the inhibition mechanism. The HOMO energies demonstrate an increasing trend from ASP (-6.89 eV) to TASP (-6.48 eV), indicating enhanced electron-donating capability with increasing molecular size. Conversely, LUMO energies shift from positive (ASP: 0.23 eV) to negative values (DASP: -0.51 eV, TASP: -0.43 eV), suggesting improved electron-accepting abilities in the larger molecules. The decreasing band gap values (ASP: 7.12 eV → DASP: 6.12 eV → TASP: 6.05 eV) indicate enhanced chemical reactivity and greater ease of electron transfer with increasing molecular size. Frontier molecular orbital diagrams of aspartic and oligomers is shown in Figure 2.

Table 1: Calculated quantum chemical parameters of Aspartic acids and its oligomers at 6-311++G(d,p) level of theory

Quantum descriptors	Aspartic Acid (ASP)	Di-Aspartic Acid (DASP)	Tri-Aspartic Acid (TASP)
E_{HOMO} (eV)	-6.89	-6.63	-6.48
E_{LUMO} (eV)	0.23	-0.51	-0.43
ΔE (eV)	7.12	6.12	6.05
η (eV)	-3.215	-3.99	-3.02
S(eV^{-1})	-0.311	-0.251	-0.33
ΔN	-0.52	-0.56	-0.59
Log P	-1.29	-2.72	-4.16
Ovality	1.26	1.42	1.57
PSA	73.32	120.87	173.15
Polarizability	48.71	56.73	64.46
E_{Solv} (kJ/mol)	-50.41	-85.17	-378.22
IP	6.89	6.83	7.08
EA	-0.23	0.57	0.43
X	3.33	3.57	3.46
ω	1.56	2.08	1.97
V	111.14	207.52	303.98
Area	140.43	240.52	343.62
DM (debye)	2.66	3.67	7.08
$\Delta E_{back\text{-}donation}$	-0.89	-0.77	-0.76
MW (amu)	117.10	232.19	347.28
Energy (au)	-437.09	-872.98	-1308.88

LUMO energy (E_{LUMO}), HOMO energy (E_{HOMO}), band gap (ΔE), *hardness* (*η*), softness (*S*),Number of electron transfer (ΔN), hydrophobicity (Log P), Polar surface area (PSA), Solvation energy (E_{solv})Ionization potential (IP), Electron affinity *(EA), electronegativity (χ), electrophilicity index (ω),* Volume *(V), Area* (A), back-donation electron donation ($\Delta E_{back\text{-}donation}$), Molecular Weight (MW)

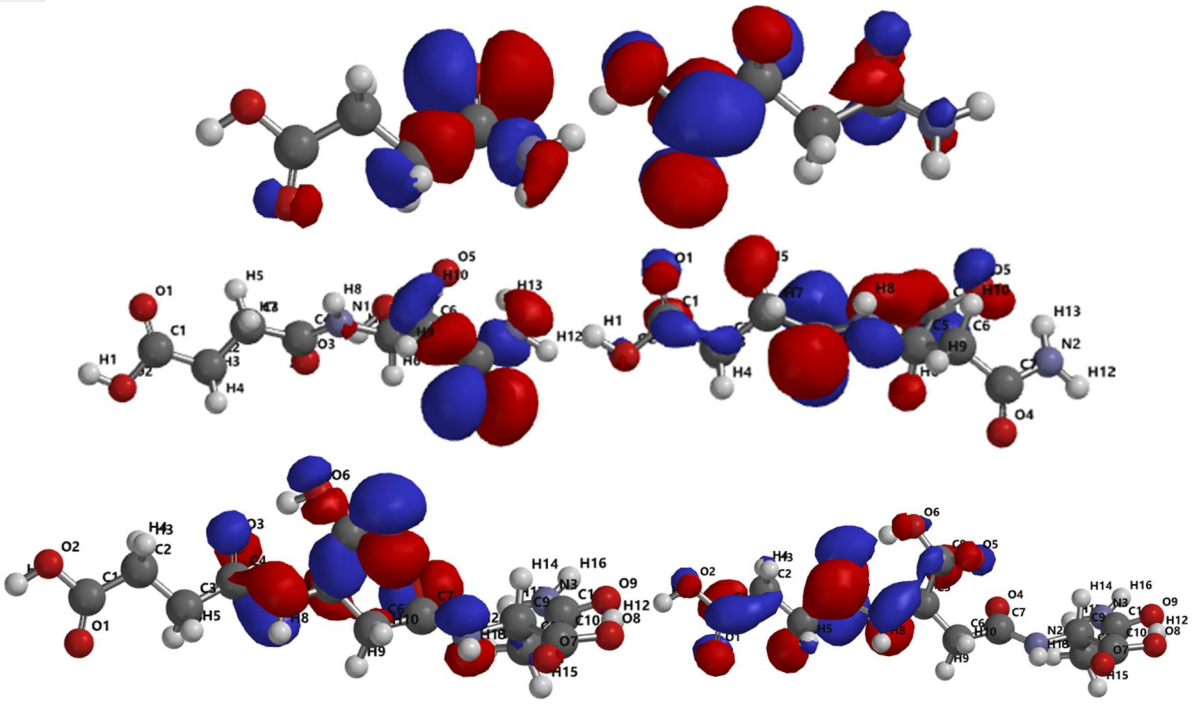

Figure 2: Frontier molecular orbitals (FMO) of aspartic acid, di-aspartic acid and tri-aspartic acid molecules calculated at 6-311++G(d,p) level of theory.

The global hardness values show variation across the series (ASP: -3.215 eV → DASP: -3.99 eV → TASP: -3.02 eV), while softness values (-0.311, -0.251, -0.33 eV^{-1} respectively) suggest flexible electronic structure adaptation during metal surface interaction. The electron transfer number (ΔN) becomes increasingly negative (ASP: -0.52 → DASP: -0.56 → TASP: -0.59), indicating enhanced electron-accepting tendency with increasing molecular size. The electrophilicity index shows optimal values for DASP (2.08) compared to ASP (1.56) and TASP (1.97), suggesting potentially superior inhibition performance.

Polar surface area and volume parameters demonstrate increases with molecular size. The polar surface area increases significantly (ASP (73.32) > DASP (120.87) > TASP (173.15), suggesting enhanced surface interaction capabilities. Dipole moment values show substantial increase (ASP (2.66) > DASP (3.67) > TASP (7.08) debye, indicating stronger electrostatic interaction potential with the metal surface. The increasingly negative solvation energies (ASP: -50.41 > DASP: -85.17 >TASP: -378.22 kJ/mol) and hydrophobicity (Log P) values (ASP: -1.29 > DASP: -2.72 > TASP: -4.16) indicate improved solubility and distribution characteristics in aqueous media.

The ionization potential remains relatively stable (6.89-7.08 eV), while electron affinity shows notable variation (ASP: -0.23 → DASP: 0.57 → TASP: 0.43). Electronegativity values exhibit slight variation (3.33-3.57), suggesting consistent electron-accepting tendencies. The back-donation electron transfer values show a slight decrease in magnitude (-0.89 → -0.77 → -0.76), indicating maintained electron-sharing capabilities despite increasing molecular size.

Molecular dimensions show predictable increases with additional monomeric units, as evidenced by volume (111.14 → 207.52 → 303.98) and surface area (140.43 → 240.52 → 343.62) measurements. Ovality values (1.26 → 1.42 → 1.57) indicate increasingly elongated structures, potentially beneficial for surface coverage.

These quantum chemical parameters collectively suggest that an increasing molecular size enhances electron transfer capabilities and improved surface interaction potential. Electronic properties indicate potentially superior inhibition performance for larger molecules while structural parameters suggest enhanced surface coverage capabilities with increasing molecular size

B. Local Reactivity and Fukui Function of ASP, DASP, and TASP molecules

The Fukui function analysis reveals significant insights into the reactive behavior of ASP, DASP, and TASP molecules. A systematic comparison of these molecules demonstrates a clear trend in the magnitude of Fukui function values, which generally decrease as molecular complexity increases. In ASP, the highest nucleophilic attack value (f_k^+ = 0.060 at C_2) is notably larger than the corresponding maximum values in DASP (f_k^+ = 0.037 at C_2) and TASP (f_k^+ = 0.027 at C_3).

This progressive reduction in Fukui function magnitudes suggests that increased molecular size may lead to more distributed electron density and potentially more moderate, but widespread, reactive capabilities.

The heteroatoms, particularly oxygen and nitrogen as shown in the optimized configurations (Figure 2), exhibit distinctive reactive patterns across all three molecules. Oxygen atoms consistently demonstrate strong electrophilic character, as evidenced by the significant negative f_k^- values (O_3: -0.252 in ASP, O_4: -0.187 in DASP, O_5: -0.094 in TASP). The nitrogen atoms display more moderate reactivity, with values ranging from -0.050 to -0.012, suggesting their secondary role in potential electron-accepting processes. This consistent pattern indicates that oxygen atoms likely serve as primary sites for electron acceptance in corrosion inhibition processes, while nitrogen atoms may provide supplementary reactive sites.

The molecular electrostatic potential (MEP) maps of the corrosion inhibitors are shown in Figure 3, The MEP surface represents the local regions on the organic systems that are susceptible to nucleophilic attack (blue region) and electrophilic attack (red, orange, yellow and green region) (Oyeneyin et al., 2021).

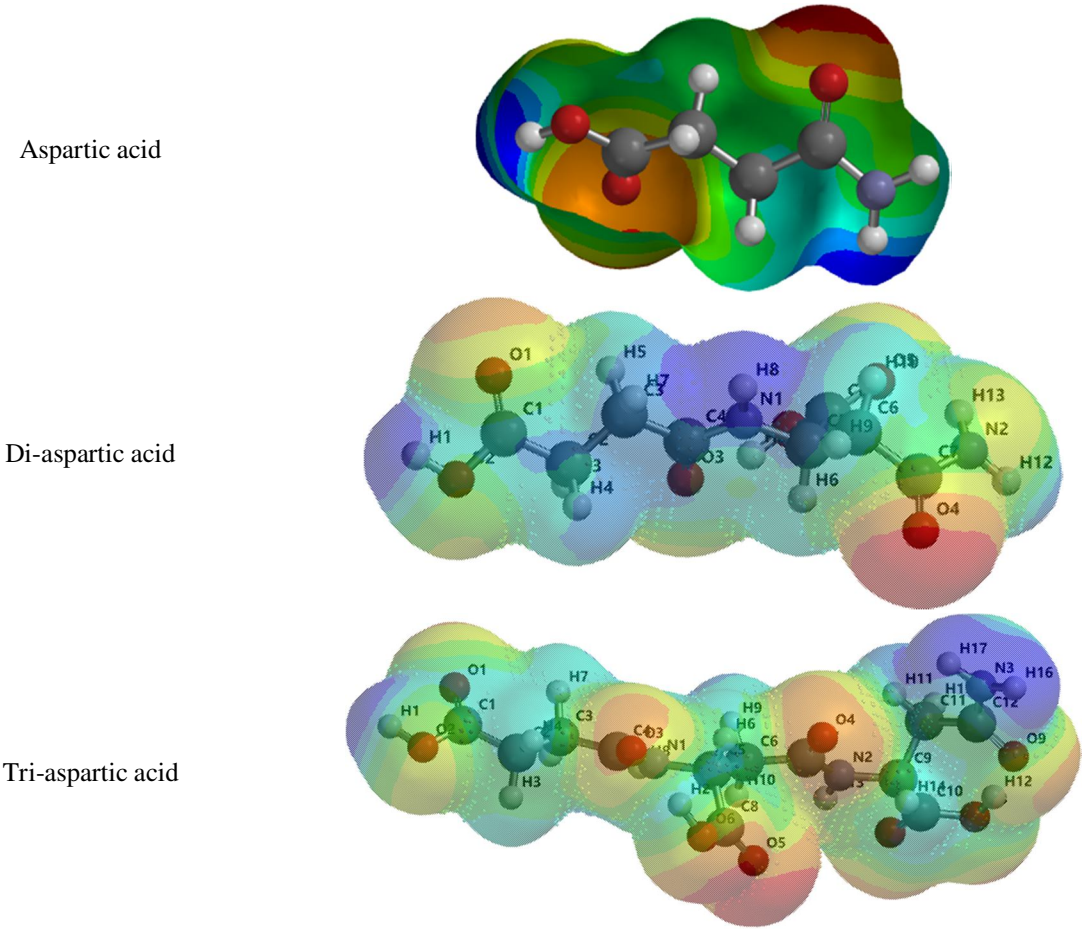

Figure 3: Molecular electrostatic potential (MEP) map of Aspartic, di-Aspartic and tri-Aspartic acids

Table 2: Selected Mulliken atomic charges and Fukui functions for ASP

Atoms	$q_k(N)$	$q_k(N-1)$	$q_k(N+1)$	f_k^+	f_k^-	$\Delta f_k(r)$
C1	0.577	0.635	0.426	-0.151	-0.058	-0.093
C2	-0.355	-0.388	-0.295	0.06	0.033	0.027
C3	-0.369	-0.391	-0.322	0.047	0.022	0.025
C4	0.598	0.655	0.494	-0.104	-0.057	-0.047
N1	-0.748	-0.698	-0.774	-0.026	-0.05	0.024
O1	-0.467	-0.316	-0.598	-0.131	-0.151	0.02
O2	-0.568	-0.511	-0.627	-0.059	-0.057	-0.002
O3	-0.504	-0.252	-0.602	-0.098	-0.252	0.154

Table 3: Selected Mulliken atomic charges and Fukui functions for DASP

Atoms	$q_k(N)$	$q_k(N-1)$	$q_k(N+1)$	f_k^+	f_k^-	$\Delta f_k(r)$
C1	0.584	0.617	0.504	-0.08	-0.033	-0.047
C2	-0.359	-0.371	-0.322	0.037	0.012	0.025
C3	-0.367	-0.387	-0.331	0.036	0.02	0.016
C4	0.643	0.655	0.554	-0.089	-0.012	-0.077
N1	-0.61	-0.587	-0.617	-0.007	-0.023	0.016
O1	-0.462	-0.374	-0.53	-0.068	-0.088	0.02
O2	-0.566	-0.533	-0.598	-0.032	-0.033	0.001
O3	-0.559	-0.509	-0.631	-0.072	-0.05	-0.022
C5	-0.075	-0.093	-0.042	0.033	0.018	0.015
C6	-0.384	-0.404	-0.36	0.024	0.02	0.004
C7	0.555	0.603	0.54	-0.015	-0.048	0.033
N2	-0.739	-0.691	-0.747	-0.008	-0.048	0.04
O4	-0.497	-0.31	-0.532	-0.035	-0.187	0.152
C8	0.625	0.655	0.545	-0.08	-0.03	-0.05
O5	-0.472	-0.42	-0.553	-0.081	-0.052	-0.029
O6	-0.58	-0.541	-0.626	-0.046	-0.039	-0.007

Table 4: Selected Mulliken atomic charges and Fukui functions for TASP

TASP	$q_k(N)$	$q_k(N-1)$	$q_k(N+1)$	f_k^+	f_k^-	$\Delta f_k(r)$
C1	0.583	0.607	0.521	-0.062	-0.024	-0.038
C2	-0.36	-0.369	-0.334	0.026	0.009	0.017
C3	-0.369	-0.383	-0.342	0.027	0.014	0.013
C4	0.638	0.647	0.571	-0.067	-0.009	-0.058
N1	-0.615	-0.592	-0.623	-0.008	-0.023	0.015
O1	-0.463	-0.408	-0.517	-0.054	-0.055	0.001
O2	-0.565	-0.544	-0.591	-0.026	-0.021	-0.005
O3	-0.554	-0.512	-0.608	-0.054	-0.042	-0.012
C5	-0.067	-0.084	-0.047	0.02	0.017	0.003
C6	-0.404	-0.414	-0.392	0.012	0.01	0.002
C7	0.659	0.667	0.649	-0.01	-0.008	-0.002
N2	-0.635	-0.608	-0.638	-0.003	-0.027	0.024
O4	-0.551	-0.468	-0.562	-0.011	-0.083	0.072
C8	0.634	0.675	0.612	-0.022	-0.041	0.019
O5	-0.461	-0.367	-0.495	-0.034	-0.094	0.06
O6	-0.592	-0.551	-0.614	-0.022	-0.041	0.019
C9	-0.049	-0.075	-0.036	0.013	0.026	-0.013
C10	0.602	0.636	0.578	-0.024	-0.034	0.01
O7	-0.473	-0.406	-0.501	-0.028	-0.067	0.039
O8	-0.591	-0.556	-0.611	-0.02	-0.035	0.015
C11	-0.389	-0.396	-0.377	0.012	0.007	0.005
C12	0.628	0.641	0.562	-0.066	-0.013	-0.053
O9	-0.54	-0.497	-0.6	-0.06	-0.043	-0.017
N3	-0.731	-0.719	-0.753	-0.022	-0.012	-0.01

C. The structural-reactivity relationships of Aspartic acid and oligomers

The structural-reactivity relationships reveal interesting patterns as monomeric units are added from ASP to TASP. The distribution of reactive sites becomes more dispersed with increasing molecular size, as evidenced by the more uniform Fukui function values in TASP compared to ASP. For instance, while ASP shows a pronounced reactive site at O3 (f_k^- = -0.252), TASP exhibits multiple moderately reactive sites (O4: -0.087, O5: -0.094, O7: -0.077), suggesting a more distributed electron density. This structural evolution appears to influence the local reactivity patterns, potentially enabling multiple points of interaction with metal surfaces during corrosion inhibition. Analysis of carbon atom reactivity reveals distinct patterns across the molecular series. The carbon atoms display variable nucleophilic character, with the highest f_k^+ values consistently observed in sp^3 carbons adjacent to electron-withdrawing groups. In ASP, C_2 exhibits the highest nucleophilic character (f_k^+ = 0.060), while DASP and TASP show relatively lower values (0.037 and 0.027, respectively) for corresponding carbons. This systematic decrease in carbon reactivity with increasing molecular size suggests a dilution effect on local electron density.

When examining the differences between nucleophilic and electrophilic attacks, the largest difference is observed at O_3 (0.154) For ASP, indicating significant variation in its ability to participate in nucleophilic versus electrophilic reactions. In DASP, O_4 shows the highest difference (0.152), similar to ASP's O_3. For TASP, the differences are generally smaller, with the maximum difference observed at O_4 (0.072). These results suggest that the oxygen atoms, particularly O_3 in ASP and O_4 in DASP, play crucial roles in the molecules' reactive behavior and likely contribute significantly to their corrosion inhibition properties. The decreasing magnitude of Fukui function values from ASP to TASP might indicate a trend in their relative reactive capabilities and potentially their effectiveness as corrosion inhibitors. The presence of multiple reactive sites, particularly the strongly electrophilic oxygen atoms (O_3 in ASP: f_k^- = -0.252; O_4 in DASP: f_k^- = -0.187) suggests a multi-point adsorption mechanism. These sites likely facilitate strong electronic interactions with the metal surface, while the more moderate reactivity of nitrogen atoms may provide additional anchoring points, potentially enhancing the overall inhibition efficiency.

Pattern analysis reveals consistent reactivity trends across functional groups. Carbonyl oxygens consistently show stronger electrophilic character compared to hydroxyl oxygens, as evidenced by their more negative f_k^- values. This recurring pattern suggests that carbonyl groups may serve as primary interaction sites for metal surface binding. The spatial distribution of these reactive sites appears optimized for surface coverage, particularly in larger molecules like TASP. Structurally,the progressive increase in molecular size from ASP to TASP corresponds with a more distributed pattern of reactive sites, potentially allowing for more adaptable surface interactions. The flexibility of the molecular backbone may facilitate optimal orientation of reactive sites during surface adsorption, maximizing inhibition effectiveness. Therefore, molecular size and flexibility significantly influence reactive site accessibility. Mechanistically, the Fukui function values support a dual-mechanism inhibition process. The presence of both strong nucleophilic (positive f_k^+ and electrophilic (negativef_k^-) sites suggests that these molecules can participate in both electron donation to and acceptance from the metal surface. This bidirectional electron transfer capability likely enhances their corrosion inhibition efficacy. However, the strong electrophilic character of oxygen atoms suggests potential pH sensitivity, as protonation states could affect their electron-accepting capabilities. Temperature variations might also impact molecular flexibility and, consequently, the accessibility of reactive sites for surface interaction.

IV. CONCLUSION

This study elucidates the molecular-level mechanisms by which aspartic acid and its oligomers inhibit iron corrosion, combining quantum chemical calculations with reactivity analyses. Oligomerization would enhance performance through cooperative interactions between polymer chains and the iron surface, facilitating dense protective film formation. Future research should investigate synergistic combinations with other eco-friendly inhibitors and scalable synthesis methods for oligomers. This research advances corrosion science by linking molecular properties to inhibition performance, offering strategies to optimize green inhibitors. It also highlights the broader potential of bio-inspired molecules in sustainable materials engineering. From a practical application perspective, these findings offer valuable guidance for inhibitor design. The observed patterns suggest that optimal inhibitor design should maintain strong electron-accepting sites (like carbonyl oxygens) while a balanced distribution of reactive sites may be more effective than concentrated reactivity.

REFERENCES

[1] El Ibrahimi, B., Jmiai, A., Bazzi, L., & El Issami, S. (2020). Amino acids and their derivatives as corrosion inhibitors for metals and alloys. Arabian Journal of Chemistry, 13(1), 740-771.

[2] Bereket, G., Hur, E., & Ogretir, C. (2002). Quantum chemical studies on some imidazole derivatives as corrosion inhibitors for iron in acidic medium. Journal of Molecular Structure: THEOCHEM, 578(1), 79-88.

[3] Chauhan, D. S., Quraishi, M. A., Srivastava, V., Haque, J., & El Ibrahimi, B. (2021). Virgin and chemically functionalized amino acids as green corrosion inhibitors: Influence of molecular structure through experimental and in silico studies. Journal of Molecular Structure, 1226(Part B), 129259.
[4] El-Hajjaji, F., Messali, M., Aljuhani, A., Aouad, M. R., Hammouti, B., Belghiti, M. E., Chauhan, D. S., & Quraishi, M. A. (2018). Pyridazinium-based ionic liquids as novel and green corrosion inhibitors of carbon steel in acid medium: Electrochemical and molecular dynamics simulation studies. Journal of Molecular Liquids, 249, 997-1008.
[5] Guo, L., Kaya, S., Obot, I. B., Zheng, X., & Qiang, Y. (2017). Toward understanding the anticorrosive mechanism of some thiourea derivatives for carbon steel corrosion: A combined DFT and molecular dynamics investigation. Journal of Colloid and Interface Science, 506, 478-485.
[6] Kumari, P., & Lavanya, M. (2024). Optimization strategies for corrosion management in industries with artificial neural network and response surface technology: A comprehensive review. Journal of Bio- and Tribo-Corrosion, 10, 59.
[7] Novák, P., Bellezze, T., Cabibbo, M., Gamsjäger, E., Wiessner, M., Rajnovic, D., Jaworska, L., Hanus, P., Shishkin, A., Goel, G., & Goel, S. (2021). Solutions of critical raw materials issues regarding iron-based alloys. Materials, 14(4), 899.
[8] Obot, I. B., & Obi-Egbedi, N. O. (2018). Anti-corrosive properties of xanthone on mild steel corrosion in sulphuric acid: Experimental and theoretical investigations. Current Applied Physics, 11(3), 382-392.
[9] Obot, I. B., Haruna, K., & Saleh, T. A. (2019). Atomistic simulation: A unique and powerful computational tool for corrosion inhibition research. Arabian Journal of Chemistry, 44, 1-32.
[10] Oyebamiji, A. K., Lasisi, B. M., Oyebamiji, E. O., Adegoke, A. K., Semire, B., & Adeleke, B. B. (2018). Theoretical evaluation of pyrazolo[3,4-d]pyrimidine-thiones analogues as corrosion inhibitors for carbon steel in hydrochloric acid. International Journal of Modern Chemistry, 10(2), 138-153.
[11] Oyeneyin, O. E., Ipinloju, N., Ojo, N. D., & Dada, D. (2021). Structural modification of ibuprofen as new NSAIDs via DFT, molecular docking and pharmacokinetics studies. International Journal of Advanced Engineering and Pure Sciences, 33(4), 614-626.
[12] Pearson, R. G. (1988). Absolute electronegativity and hardness: Application to inorganic chemistry. Inorganic Chemistry, 27(4), 734-740.
[13] Yadav, S., Raman, A. P. S., Singh, M. B., Massey, I., Singh, P., Verma, C., & AlFantazi, A. (2024). Green nanoparticles for advanced corrosion protection: Current perspectives and future prospects. Applied Surface Science Advances, 21, 100605.
[14] Verma, C., Quraishi, M. A., Alfantazi, A., & Rhee, K. Y. (2023). Biodegradable synthetic polymers in sustainable corrosion protection: Present and future scenarios. Advanced Industrial and Engineering Polymer Research, 6(4), 407-435.
[15] Wazzan, N. A., & Mahgoub, F. M. (2014). DFT calculations for corrosion inhibition of ferrous alloys by pyrazolopyrimidine derivatives. Open Journal of Physical Chemistry, 4(1), 6-14.
[16] Zhang, K., Yang, W., Xu, B., Chen, Y., Yin, X., Liu, Y., & Zuo, H. (2018). Amino acids modified konjac glucomannan as green corrosion inhibitors for mild steel in HCl solution. Carbohydrate Polymers, 215, 236-246.
[17] Koch, G., Varney, J., Thompson, N., Moghissi, O., Gould, M., & Payer, J. (2016). International measures of prevention, application, and economics of corrosion technologies study. NACE International.

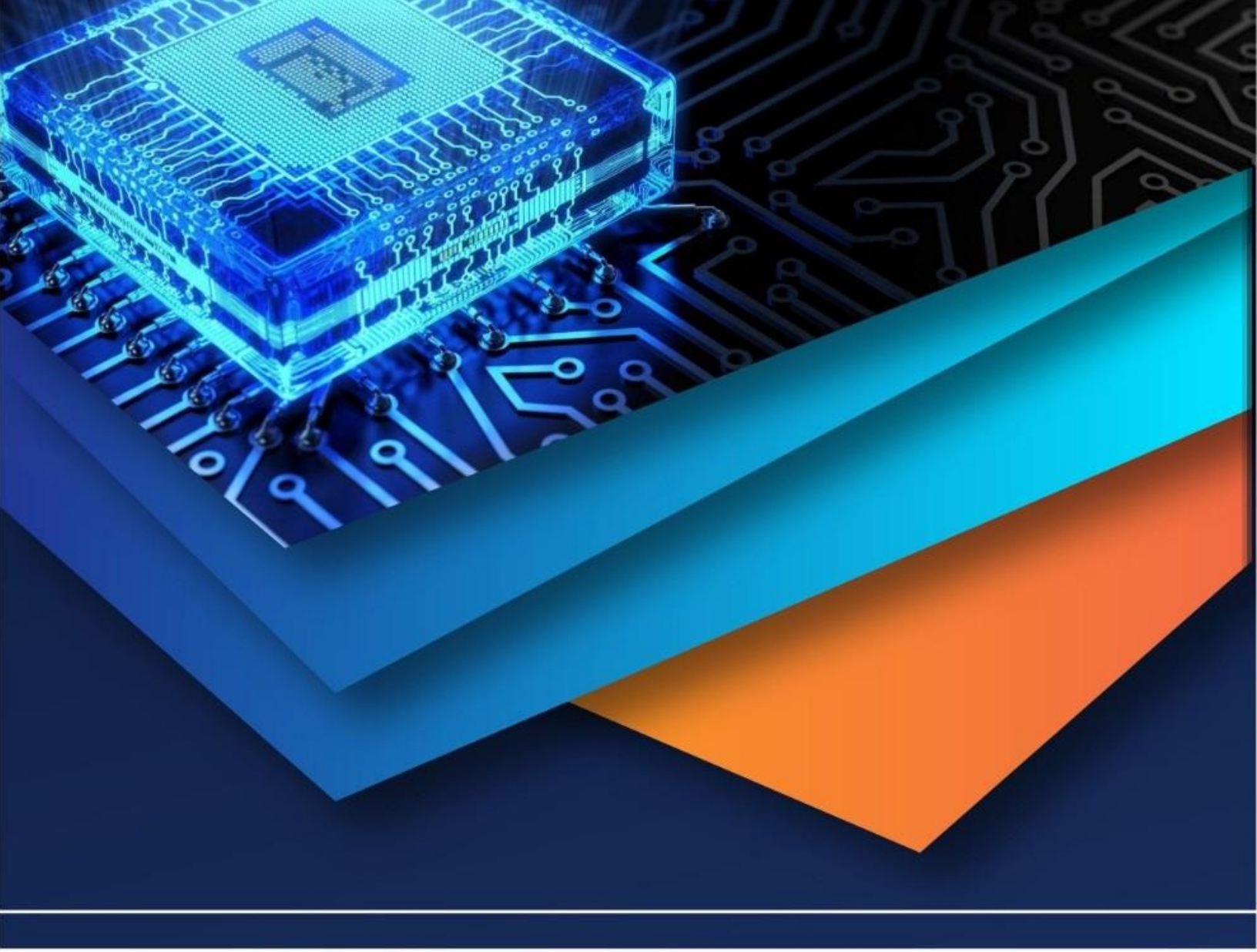

10.22214/IJRASET

45.98

IMPACT FACTOR: 7.129

IMPACT FACTOR: 7.429

INTERNATIONAL JOURNAL FOR RESEARCH

IN APPLIED SCIENCE & ENGINEERING TECHNOLOGY